Cell, Volume *189*

Supplemental information

mRNA 3′ UTRs chaperone intrinsically disordered regions to control protein activity

Yang Luo, Yaofeng Zhong, Sudipto Basu, Ming-Chung Wu, and Christine Mayr

Figure S1

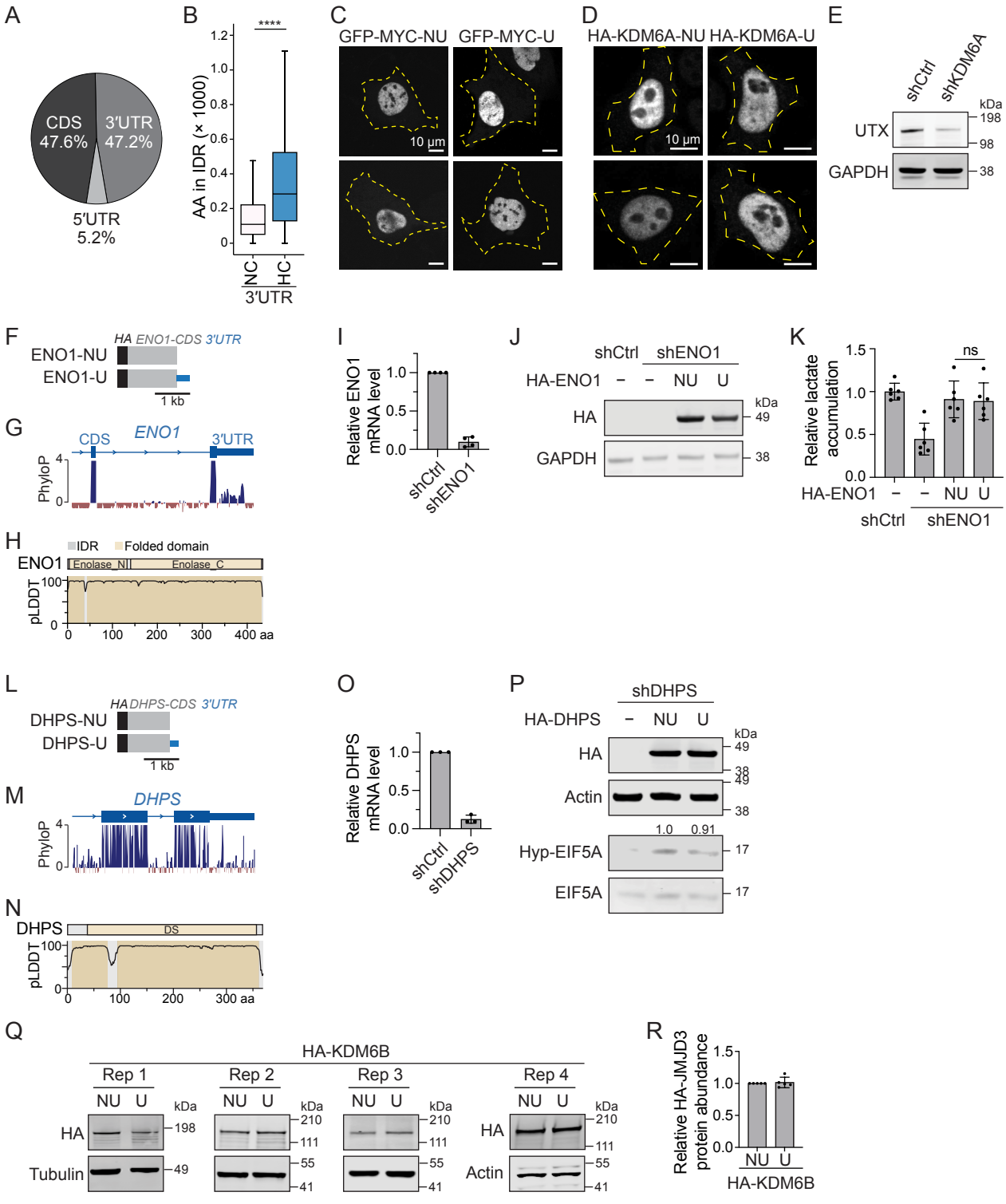
A
CDS 47.6%
3′UTR 47.2%
5′UTR 5.2%
B
****
AA in IDR (× 1000)
NC
HC
3′UTR
C
GFP-MYC-NU
GFP-MYC-U
10 μm
D
HA-KDM6A-NU
HA-KDM6A-U
10 μm
E
shCtrl
shKDM6A
kDa
UTX
198
98
GAPDH
38
F
HA ENO1-CDS 3′UTR
ENO1-NU
ENO1-U
1 kb
G
CDS
ENO1
3′UTR
PhyloP
H
IDR
Folded domain
ENO1
Enolase_NII
Enolase_C
pLDDT
400 aa
I
Relative ENO1 mRNA level
shCtrl
shENO1
J
shCtrl
shENO1
HA-ENO1
NU
U
HA
GAPDH
kDa
49
38
K
Relative lactate accumulation
ns
HA-ENO1
shCtrl
shENO1
L
HA DHPS-CDS 3′UTR
DHPS-NU
DHPS-U
1 kb
M
DHPS
PhyloP
N
DHPS
DS
pLDDT
300 aa
O
Relative DHPS mRNA level
shCtrl
shDHPS
P
shDHPS
HA-DHPS
HA
Actin
1.0
0.91
Hyp-EIF5A
EIF5A
Q
HA-KDM6B
Rep 1
Rep 2
Rep 3
Rep 4
NU
U
kDa
HA
Tubulin
Actin
198
210
111
55
49
41
R
Relative HA-JMJD3 protein abundance
HA-KDM6B

Figure S1. NC 3′UTRs in mRNA templates do not alter the activity of proteins encoded by the mRNA, related to Figure 1

A. Proportion of nucleotides assigned to 5′UTRs, CDS, and 3′UTRs in human mRNAs (N = 19,556)[2].

B. As in Fig. 1C but shown is the number of residues in IDRs based on classification using pLDDT scores from AlphaFold2. IDRs are defined as pLDDT < 80. Mann-Whitney test, $P = 5.5 \times 10^{-248}$.

C. Live-cell fluorescence microscopy of GFP-MYC-NU or GFP-MYC-U in U2OS cells. Representative image is shown. The yellow dotted line indicates the cell outline. MYC protein localizes to the nucleus in a 3′UTR-independent manner.

D. As in (C), but anti-HA immunofluorescence staining of transfected HA-KDM6A-NU or HA-KDM6A-U in MCF7 cells.

E. Western blot of endogenous UTX/KDM6A levels in MCF7 cells stably expressing either a control shRNA or an shRNA targeting KDM6A. GAPDH was used as loading control.

F. cDNA vector constructs used for ENO1 activity assays in cells, showing the HA-tag (black), CDS (gray) and full-length 3′UTR (blue).

G. PhyloP100way track of the last two exons of the *ENO1* gene.

H. Prediction of ENO1 folded domains (pLDDT ≥ 80, brown) and IDRs (pLDDT < 80, gray) using AlphaFold2 pLDDT scores. Names of annotated protein domains are given.

I. Quantification of shRNA-mediated ENO1 knockdown by qRT-PCR. Data are normalized to *RPLP0* and are represented relative to cells transduced with a scrambled shRNA (shCtrl). Data and error bars indicate mean ± SD of 4 biological replicates.

J. Western blot analysis after transfection of constructs shown in (F) into HeLa cells depleted of ENO1. GAPDH was used as a loading control.

K. Comparison of the cellular activity of ENO1 expressed from NU or U constructs in HeLa cells, indirectly measured by the accumulation of lactate in the medium. Data and error bars indicate mean ± SD of 6 biological replicates. Two-tailed t-test: ns.

L. As in (F), but DHPS expression constructs are shown.

M. As in (G), but the PhyloP track of DHPS is shown.

N. As in (H), but DHPS pLDDT values and domains are shown.

O. As in (I), but the knockdown efficiency of DHPS in HeLa cells was analyzed.

P. Comparison of DHPS cellular activity by measuring EIF5A hypusination levels via western blot. Endogenous DHPS was knocked down in HeLa cells using shRNA to evaluate the effect of transfected DHPS constructs. The relative EIF5A hypusination level was calculated by normalizing the hypusination band intensity to total EIF5A protein and is displayed above the blot.

Q. Additional independent western blot replicates showing transfected HA-tagged JMJD3/KDM6B levels in HeLa cells, as shown in Fig. 1I. Tubulin or actin was used as loading control.

R. Quantification of the HA-JMJD3 band intensity in (Q) and Fig. 1I, normalized to the loading control. Data and error bars indicate mean ± SD.

Figure S2

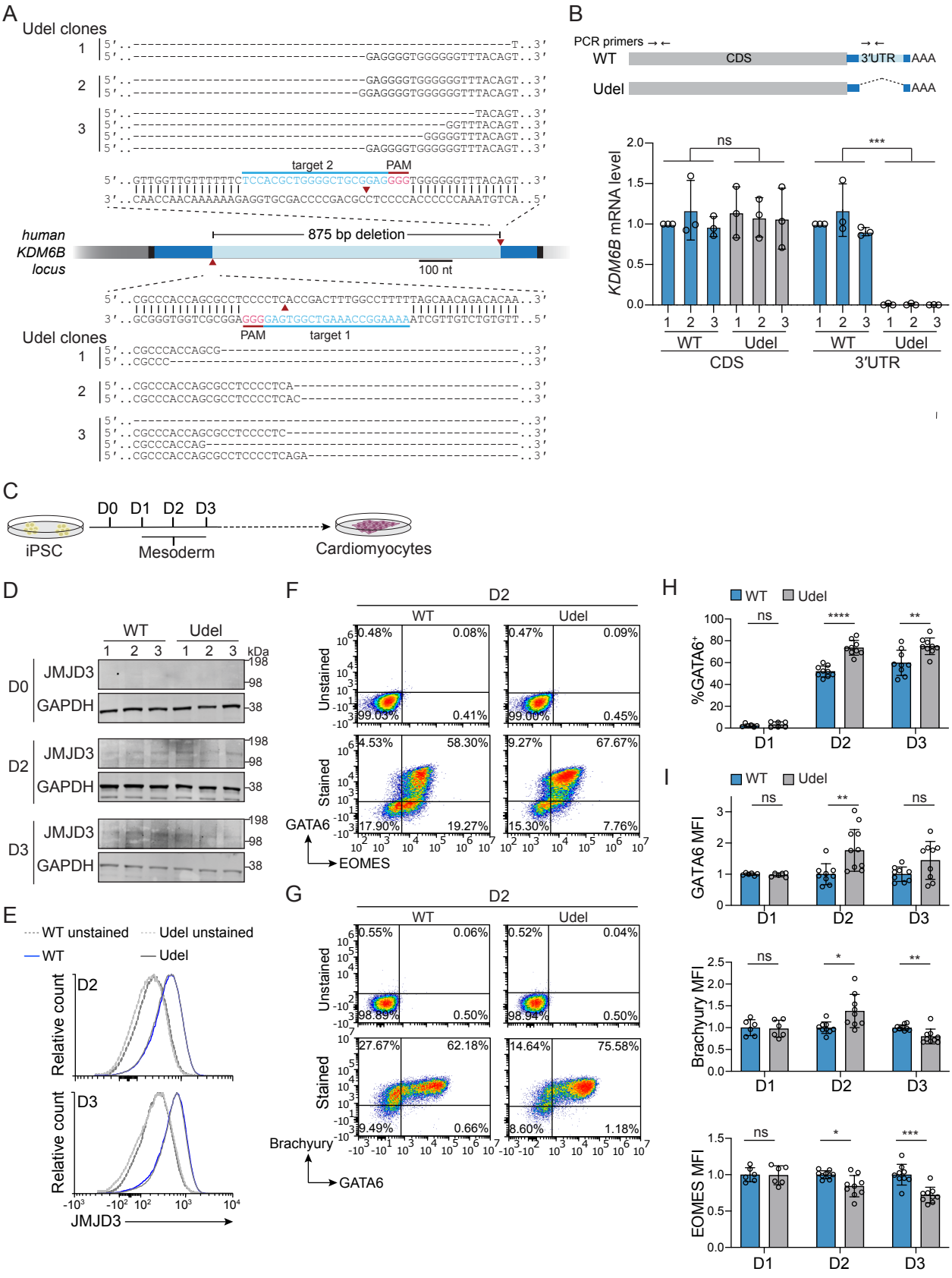
A
Udel clones
target 2
PAM
human KDM6B locus
875 bp deletion
100 nt
PAM
target 1
B
PCR primers
WT
CDS
3′UTR
AAA
Udel
KDM6B mRNA level
ns
***
CDS
3′UTR
C
D0 D1 D2 D3
iPSC
Mesoderm
Cardiomyocytes
D
WT
Udel
JMJD3
GAPDH
kDa
E
WT unstained
Udel unstained
Relative count
JMJD3
F
D2
Unstained
Stained
GATA6
EOMES
G
Brachyury
GATA6
H
%GATA6+
I
GATA6 MFI
Brachyury MFI
EOMES MFI

Figure S2. Partial deletion of the endogenous *KDM6B* 3′UTR affects mesendoderm differentiation, related to Figure 1

A. Sequences of the human *KDM6B* locus targeted by Cas9 and guide RNAs. The genomic sequence deleted in *KDM6B* 3′UTR deletion cells (Udel) is shown in skyblue. sgRNA target sites and PAMs are indicated by blue and magenta bars, respectively, and predicted cutting sites are marked by a red triangle. Sequence alignment of KDM6B alleles spanning the deletion sites in Udel iPSC cell clones obtained from amplicon sequencing are shown.

B. *KDM6B* mRNA expression measured by qRT-PCR with a primer pair located in the CDS or 3′UTR in the indicated samples derived from iPSC cells. Data are shown as mean ± SD of 3 biological replicates. WT, wild type. T-test for independent samples: ***, $P < 0.001$; ns, not significant.

C. Schematic for in vitro cardiomyocyte differentiation using the GiWi protocol. The cells adopt mesoderm and mesendoderm markers at d2 and d3, which was analyzed here.

D. Western blot of endogenous JMJD3 protein in WT and Udel iPSC clones at day 0, day 2, and day 3 of the differentiation protocol. GAPDH was used as the loading control.

E. Representative flow cytometry analysis of endogenous JMJD3 protein expression WT and Udel iPSC clones at day 2 and day 3 of the differentiation protocol.

F. Representative flow cytometry plots at day 2 of the differentiation protocol, analyzing the percent of GATA6- and EOMES-positive cells in the indicated samples.

G. As in (F), but the percent of Brachyury- and GATA6-positive cells is shown.

H. Quantification of day 1-3 flow cytometry data for percent GATA6-positive cells is shown as mean ± SD of $N = 3$ biological replicates for each of the three WT and Udel clones. Two-tailed t-test, ns, not significant; **, $P = 0.005$; ****, $P < 0.0001$.

I. As in (H), but mean fluorescence intensity (MFI) as measure of protein expression of GATA6, Brachyury, and EOMES is shown as mean ± SD obtained from 3 biological replicates each for three WT and three Udel clones. Two-tailed t-test: ns, not significant; *, $P < 0.05$; **, $P < 0.01$; ***, $P < 0.001$.

Figure S3

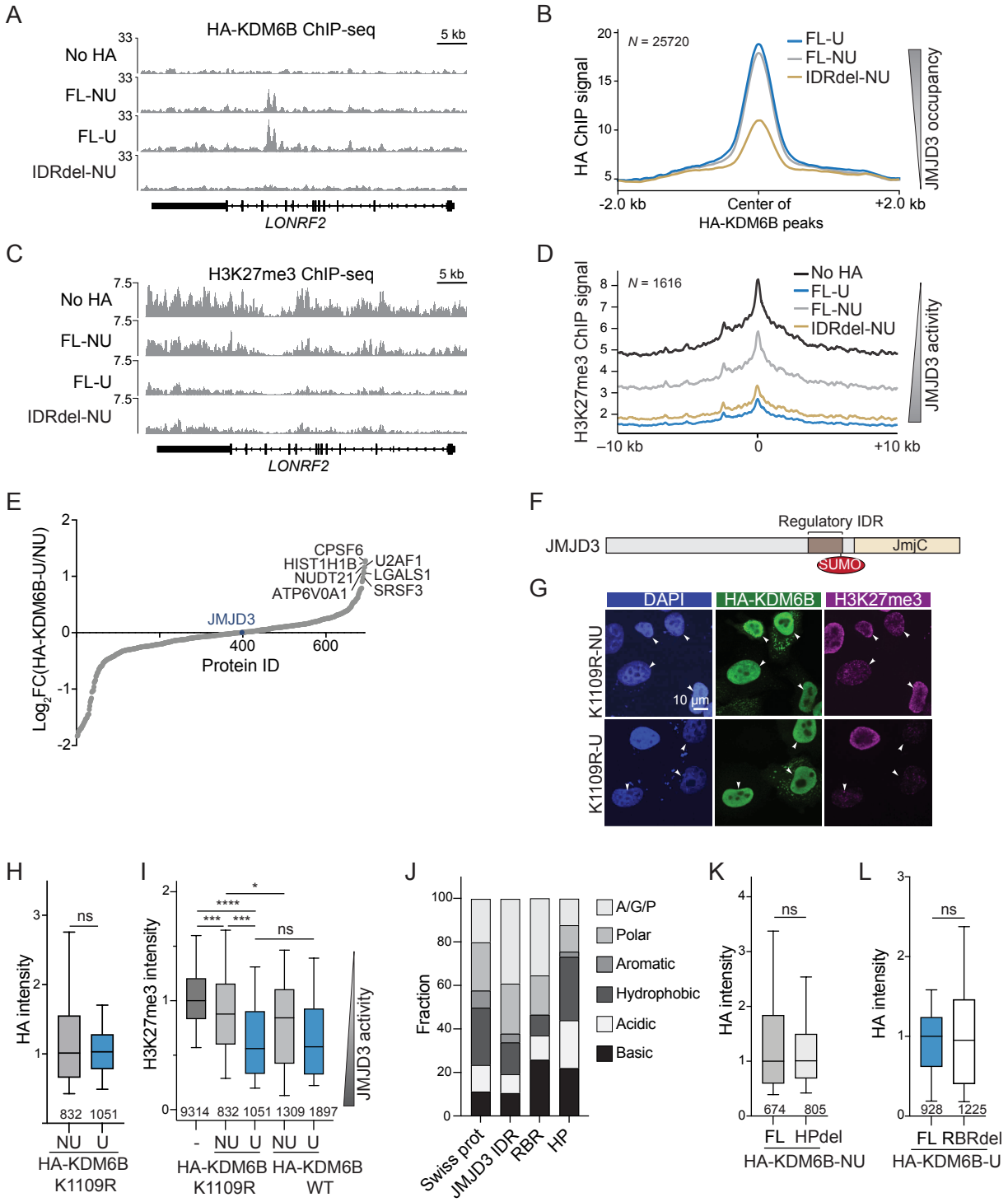
A
HA-KDM6B ChIP-seq
5 kb
No HA
FL-NU
FL-U
IDRdel-NU
LONRF2
B
N = 25720
FL-U
FL-NU
IDRdel-NU
HA ChIP signal
JMJD3 occupancy
-2.0 kb
Center of
HA-KDM6B peaks
+2.0 kb
C
H3K27me3 ChIP-seq
5 kb
No HA
FL-NU
FL-U
IDRdel-NU
LONRF2
D
N = 1616
No HA
FL-U
FL-NU
IDRdel-NU
H3K27me3 ChIP signal
JMJD3 activity
–10 kb
0
+10 kb
E
CPSF6
HIST1H1B
NUDT21
ATP6V0A1
U2AF1
LGALS1
SRSF3
JMJD3
Protein ID
F
Regulatory IDR
JMJD3
JmjC
SUMO
G
DAPI
HA-KDM6B
H3K27me3
K1109R-NU
K1109R-U
10 μm
H
HA intensity
ns
832 1051
NU U
HA-KDM6B
K1109R
I
H3K27me3 intensity
JMJD3 activity
9314 832 1051 1309 1897
- NU U NU U
HA-KDM6B K1109R
HA-KDM6B WT
J
Fraction
A/G/P
Polar
Aromatic
Hydrophobic
Acidic
Basic
Swiss prot
JMJD3 IDR
RBR
HP
K
HA intensity
ns
674 805
FL HPdel
HA-KDM6B-NU
L
HA intensity
ns
928 1225
FL RBRdel
HA-KDM6B-U

Figure S3. The JMJD3 IDR mediates 3'UTR-dependent activity regulation independently of its roles in chromatin occupancy and SUMOylation, related to Figure 2 and 3

A. Genome browser view of genomic context of *LONRF2* for anti-HA ChIP-seq signal is shown. ChIP-seq was performed after transfection of the indicated KDM6B constructs, shown in Fig. 1H and 2B. No HA indicates negative control.

B. Metaplot analysis of experiment from (A) using all anti-HA ChIP-seq peaks with $P < 0.001$.

C. As in (A), but spike-in normalized anti-H3K27me3 ChIP-seq signal is shown.

D. Metaplot analysis of experiment from (C) using all anti-H3K27me3 ChIP-seq peaks with $P < 0.001$ that showed at least a 50% signal reduction in KDM6B-U transfected samples compared to the control.

E. Analysis of the 3′UTR-dependence of JMJD3 interaction partners using SILAC-based co-IP MS. Shown is the log2 fold change (FC) of protein counts of samples expressing HA-KDM6B-NU or -U. Only proteins with at least two unique peptides identified are included.

F. Schematic representation of the annotated SUMOylation site within the regulatory IDR. To examine if 3′UTR regulates JMJD3 activity via SUMOylation at this site, K1109 was mutated into R to abolish SUMOylation while maintaining the positive charge.

G. As in Fig. 1L, but JMJD3 cellular activity in HeLa cells after transfection of the K1109R mutant constructs.

H. As in Fig. 1M, but JMJD3 protein abundance of the K1109R constructs was measured as HA intensity from $N = 3$ independent experiments. Mann-Whitney test: ns, not significant.

I. As in Fig. 1N, but the cellular activity of wildtype JMJD3 and K1109R were measured as reduction in H3K27me3. Normalized H3K27me3 intensity values obtained from $N = 3$ independent experiments. Mann-Whitney test: ****, $P < 10^{-204}$; ***, $P < 10^{-24}$; *, $P < 10^{-6}$; ns, not significant.

J. Stacked bar chart showing the relative fractions of each amino acid category across all proteins in the Swiss-Prot database, the JMJD3 IDR, the RBR, and the HP region, respectively.

K. As in Fig. 1M, but JMJD3 protein abundance of full-length and HPdel was measured as HA intensity from $N = 3$ independent experiments. Mann-Whitney test: ns, not significant.

L. As in Fig. 1M, but JMJD3 protein abundance of full-length and RBRdel was measured as HA intensity from $N = 3$ independent experiments. Mann-Whitney test: ns, not significant.

Figure S4

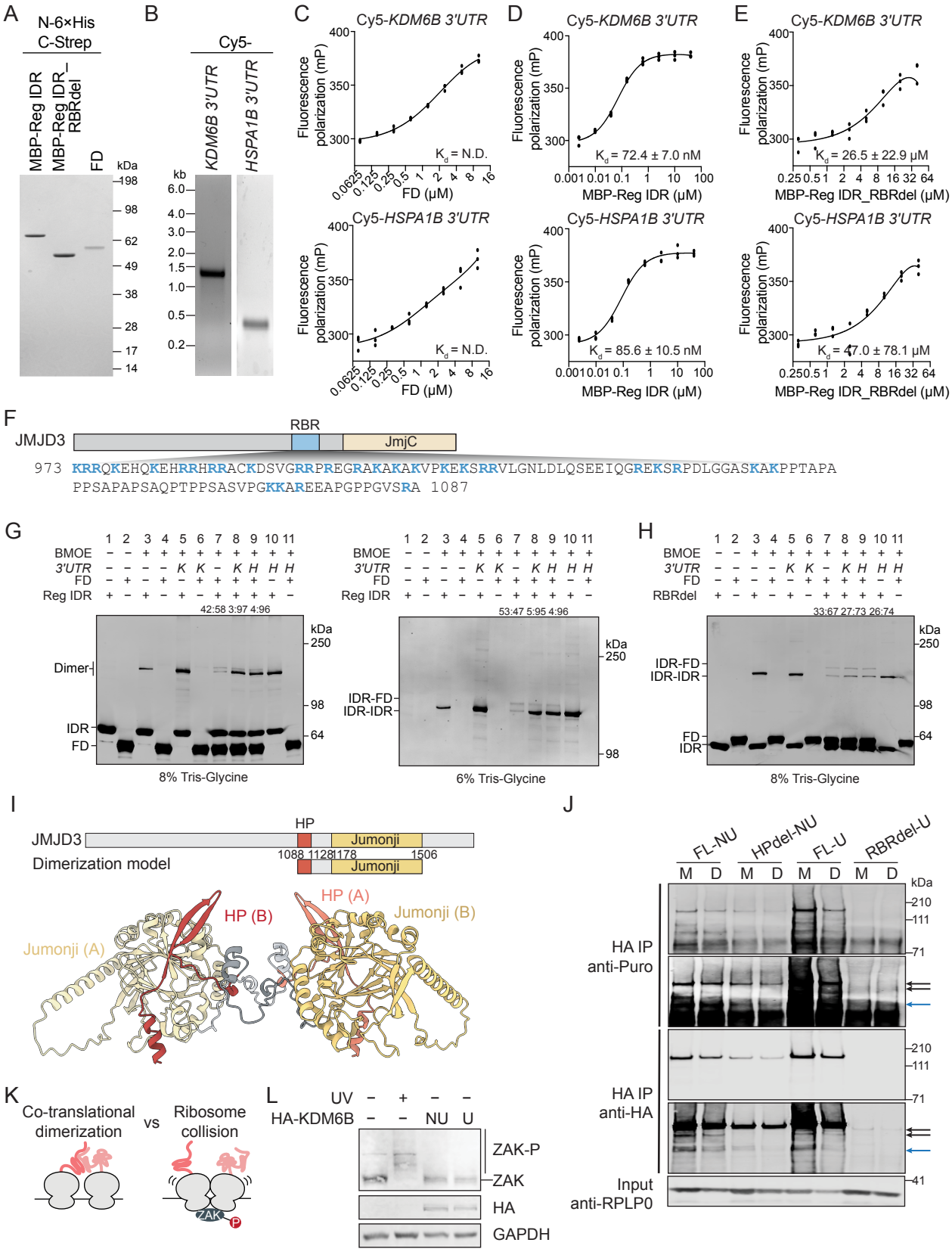
A
N-6×His
C-Strep
MBP-Reg IDR
MBP-Reg IDR_RBRdel
FD
kDa
198
98
62
49
38
28
17
14
B
Cy5-
KDM6B 3'UTR
HSPA1B 3'UTR
kb
6.0
4.0
3.0
2.0
1.5
1.0
0.5
0.2
C
Cy5-KDM6B 3'UTR
Fluorescence polarization (mP)
Kd = N.D.
FD (μM)
Cy5-HSPA1B 3'UTR
Kd = N.D.
FD (μM)
D
Cy5-KDM6B 3'UTR
Kd = 72.4 ± 7.0 nM
MBP-Reg IDR (μM)
Cy5-HSPA1B 3'UTR
Kd = 85.6 ± 10.5 nM
MBP-Reg IDR (μM)
E
Cy5-KDM6B 3'UTR
Kd = 26.5 ± 22.9 μM
MBP-Reg IDR_RBRdel (μM)
Cy5-HSPA1B 3'UTR
Kd = 47.0 ± 78.1 μM
MBP-Reg IDR_RBRdel (μM)
F
JMJD3
RBR
JmjC
973 KRRQKEHQKEHRRHRRACKDSVGRRPREGRAKAKAKVPKEKSRRVLGNLDLQSEEIQGREKSRPDLGGASKAKPPTAPA
PPSAPAPSAQPTPPSASVPGKKAREEAPGPPGVSRA 1087
G
BMOE
3'UTR
FD
Reg IDR
42:58 3:97 4:96
Dimer
IDR
FD
kDa
250
98
64
8% Tris-Glycine
53:47 5:95 4:96
IDR-FD
IDR-IDR
6% Tris-Glycine
H
RBRdel
33:67 27:73 26:74
IDR-FD
IDR-IDR
FD
IDR
8% Tris-Glycine
I
HP
JMJD3
Jumonji
1088 1128 1178 1506
Dimerization model
HP (A)
HP (B)
Jumonji (A)
Jumonji (B)
J
FL-NU
HPdel-NU
FL-U
RBRdel-U
M D M D M D M D
kDa
210
111
71
HA IP
anti-Puro
HA IP
anti-HA
Input
anti-RPLP0
41
K
Co-translational dimerization
vs
Ribosome collision
ZAK
P
L
UV
HA-KDM6B
NU U
ZAK-P
ZAK
HA
GAPDH

Figure S4. RNAs bind the JMJD3 IDR, regulating inter-domain interactions in vitro and controlling co-translational JMJD3 dimerization in cells, related to Figure 4

A. Coomassie-stained SDS–PAGE showing recombinant MBP-tagged regulatory IDR, MBP-tagged RBR-deleted regulatory IDR (RBRdel), and folded domain (FD) from JMJD3. All proteins contain a N-terminal 6xHis and a C-terminal Strep tag II.

B. Agarose gel showing in vitro transcribed Cy5-labeled *KDM6B* (1164 nt) and *HSPA1B* 3′UTRs (378 nt). The first 110 nt of the *KDM6B* 3′UTR are GC-rich and were removed to allow transcription.

C-E. Fluorescence polarization assay to measure RNA-protein interactions. Top: As RNA, the Cy5-labeled *KDM6B* 3′UTR (1164 nt) was used. Bottom: As RNA, the *HSPA1B* 3′UTR (378 nt) was used. Fluorescence polarization values obtained from $N = 3$ independent experiments are shown. The values were fitted to a sigmoidal binding curve, and the K_d was calculated in Prism using the one-site binding model. The dissociation constant (K_d) is reported as ± error of fitting.

F. Amino acid sequence of the RNA-binding region (RBR) in JMJD3. Basic residues are highlighted in blue.

G. The uncropped blot showing RNA-dependent protein-protein interactions generated through thiol-thiol crosslinking between recombinant JMJD3 regulatory IDR and FD by BMOE-mediated thiol-thiol crosslinking. The same reactions were resolved on either an 8% (left) or 6% (right) Tris-Glycine gel to allow clear visualization of individual monomer and dimer bands, respectively. *K*, *KDM6B* 3′UTR was used; *H*, *HSPA1B* 3′UTR was used as RNA.

H. As in (G) but showing the crosslinking experiment between RBRdel and FD.

I. AlphaFold3 prediction of full-length JMJD3 homodimer but shown are only the interacting domains (aa 1086-1510), color-coded as in the protein model shown above. Red, HP region; brown, Jumonji domain. (A) and (B) indicate two different JMJD3 molecules.

J. Representative immunoblots of the co-translational disome assay. Shown is the abundance of newly synthesized nascent chains derived from various HA-tagged KDM6B constructs in either the monosome (M) or disome (D) fractions obtained by sucrose gradient centrifugation after their transfection into HeLa cells. As input, RPLP0 in each M or D fraction was blotted and used for normalization purposes. Puro, puromycin. Black arrows indicate the nascent chains that overlap with the full-length HA-KDM6B bands, which were used for quantification. The blue arrow indicates a lower molecular weight, HA-tagged nascent chain that displayed a similar trend as the full-length band.

K. Disomes can form from interactions between nascent chains (left) or from ribosome collisions induced by stress (right).

L. Western blot of Phos-tag gels for ZAK phosphorylation in HeLa cells subjected to the indicated treatment.

Figure S5

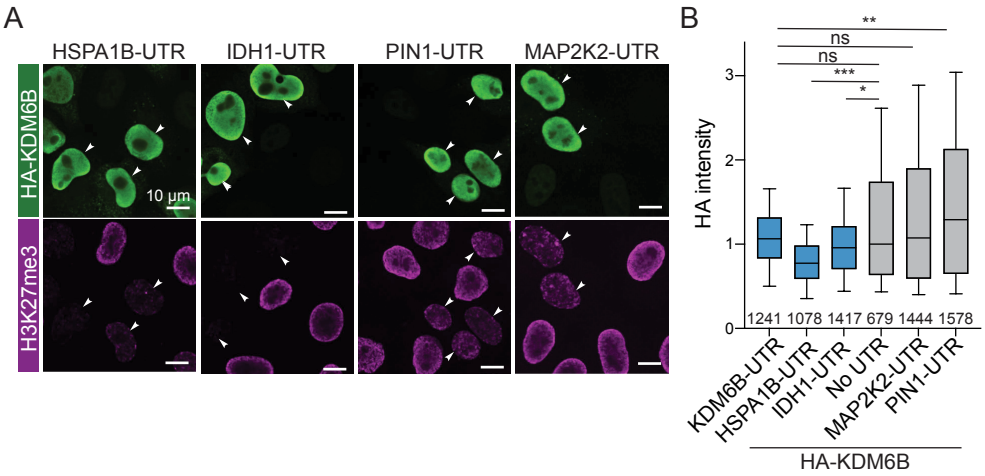

C

	Motif	Frequency FC (HC/NC 3′UTR)
1	TGTACA	1.6883
2	TTTTAA	1.54026
3	TTTAAA	1.52216
4	CCTTTT	1.49421
5	TTTTTT	1.43041
6	TATATA	1.41928
7	TATTTA	1.39787
8	GCTGTA	1.38805
9	GTTTGG	1.37004
10	GTGTGT	1.3424
11	AAAAAG	1.30467
12	GGGGGG	1.19036
13	TATCTT	1.18906
14	AAAAAA	1.18108
15	GCCGTA	1.18091

D

	Motif	Frequency FC (NC/HC 3′UTR)
1	CGCCTG	2.139137
2	GGCTCA	2.024479
3	AGGCTG	1.999364
4	GCTGGG	1.991511
5	GCCTCC	1.929698
6	GTCTCG	1.904532
7	TGAGCC	1.819749
8	CACCTG	1.711468
9	TGGGAG	1.670552
10	TAATCC	1.66157
11	GGGCCC	1.634249
12	GGCAAC	1.60031
13	GGCACC	1.581714
14	TGCCTG	1.549767
15	GATTAC	1.543643

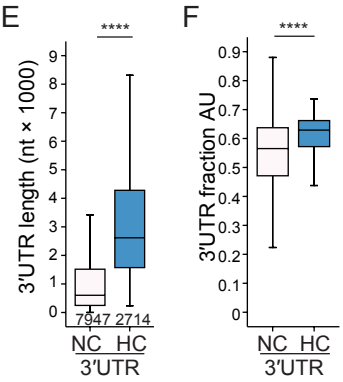

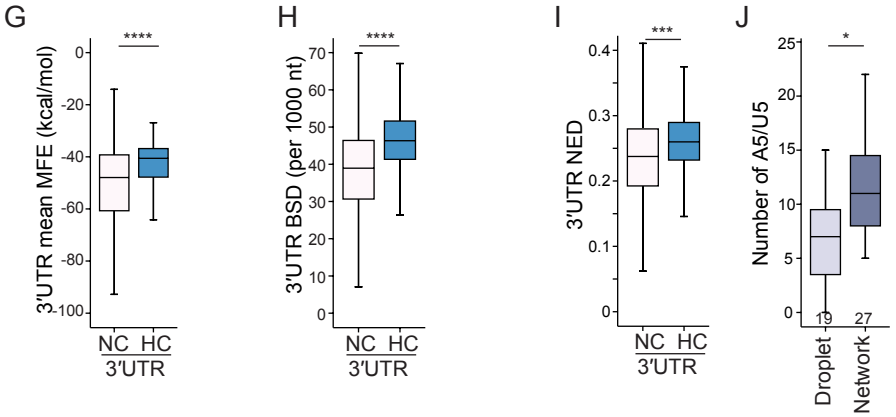

Figure S5. HC 3′UTRs are multivalent, a feature that correlates with IDR chaperone activity, related to Figure 5

A. Immunofluorescence assay to assess 3′UTR-dependent JMJD3 activity in HeLa cells after transfecting the indicated 3′UTR-swapped constructs.

B. Quantification of transfected JMJD3 abundance as HA intensity values from (A). Shown are boxplots generated from *N* = 3 independent experiments. Mann-Whitney test: ns, not significant; *, $P = 1.3 \times 10^{-5}$; **, $P = 6.9 \times 10^{-15}$; ***, $P = 1.2 \times 10^{-29}$.

C. The top 15 6-mer motifs significantly enriched in HC vs. NC 3′UTRs.

D. As in (C), but motifs enriched in the NC compared to HC 3′UTRs are shown.

E. 3′UTR length distribution of human mRNAs in HC 3′UTRs (*N* = 2714) vs NC 3′UTRs (*N* = 7947), Mann-Whitney test, *P* = 0.

F. As in (E), but AU content in 3′UTRs is shown. Mann-Whitney test, $P = 2.6 \times 10^{-130}$.

G. As in (E), but mean minimum free energy (MFE) of 3′UTRs is shown. Mann-Whitney test, $P = 8.5 \times 10^{-106}$.

H. As in (E), but RNA-RNA binding site density (BSD) in 3′UTRs is shown. Mann-Whitney test, $P = 3.6 \times 10^{-228}$.

I. As in (E), but normalized ensemble diversity (NED) values of the 3′UTRs are shown. Mann-Whitney test, $P = 4.9 \times 10^{-68}$.

J. A/U homopolymers in 3′UTRs that induced droplet-like (*N* = 19) or meshlike condensates (*N* = 27) in vitro, obtained from Ma et al., Elife (2021)[12]. Mann-Whitney test, *P* = 0.018.

Figure S6

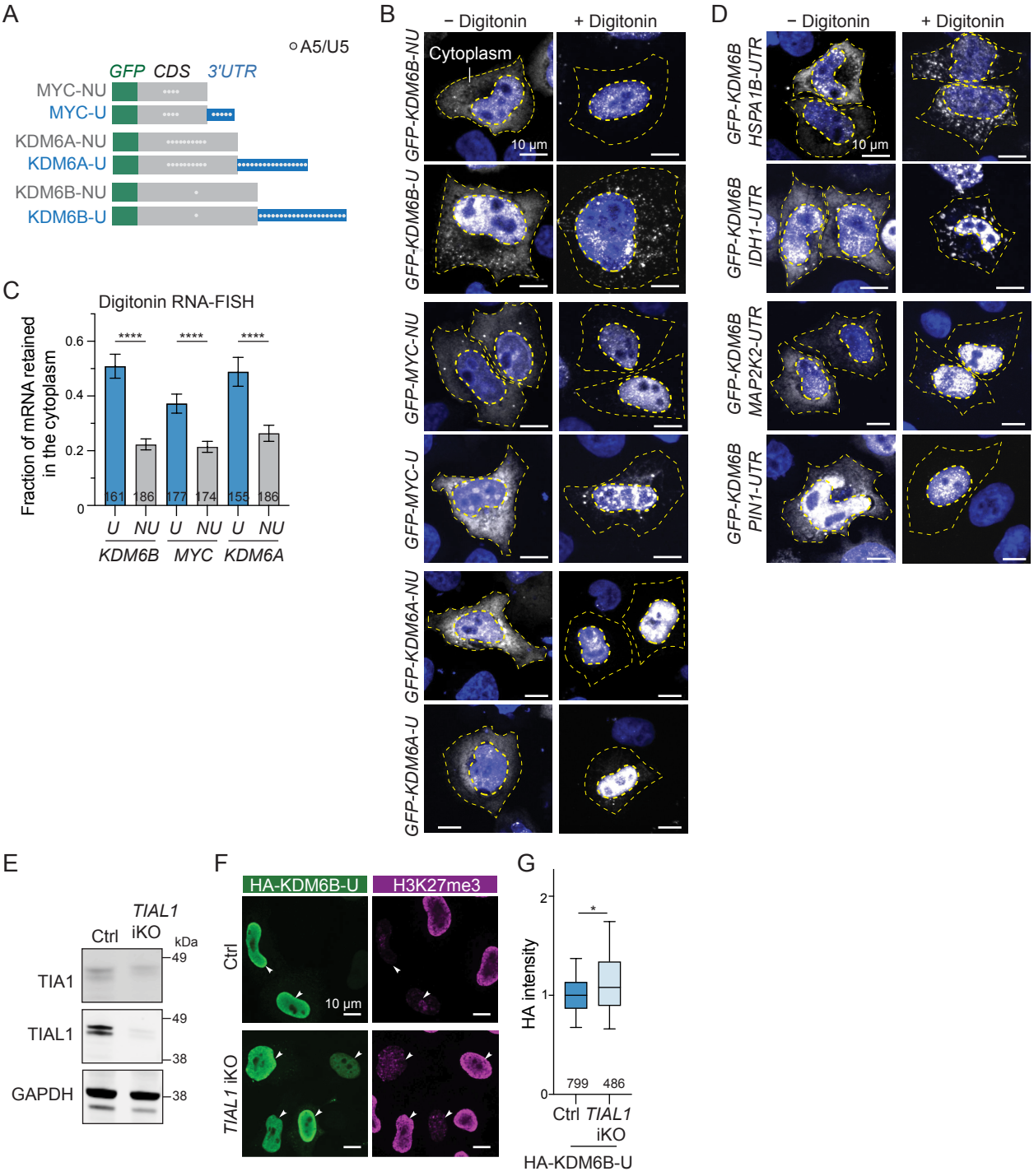
A
A5/U5
GFP CDS 3'UTR
MYC-NU
MYC-U
KDM6A-NU
KDM6A-U
KDM6B-NU
KDM6B-U
B
− Digitonin
+ Digitonin
Cytoplasm
10 µm
GFP-KDM6B-NU
GFP-KDM6B-U
GFP-MYC-NU
GFP-MYC-U
GFP-KDM6A-NU
GFP-KDM6A-U
C
Digitonin RNA-FISH
Fraction of mRNA retained in the cytoplasm
****
0.6
0.4
0.2
0
161 186 177 174 155 186
U NU U NU U NU
KDM6B MYC KDM6A
D
− Digitonin
+ Digitonin
GFP-KDM6B HSPA1B-UTR
GFP-KDM6B IDH1-UTR
GFP-KDM6B MAP2K2-UTR
GFP-KDM6B PIN1-UTR
10 µm
E
TIAL1
Ctrl iKO
kDa
TIA1
TIAL1
GAPDH
49
49
38
38
F
HA-KDM6B-U
H3K27me3
Ctrl
TIAL1 iKO
10 µm
G
HA intensity
*
2
1
0
799 486
Ctrl TIAL1 iKO
HA-KDM6B-U

Figure S6. Multivalent 3′UTRs are necessary for mRNA enrichment in meshlike condensates, related to Figure 5

A. GFP-tagged constructs used for RNA-FISH. The white dots indicate A/U homopolymers and serve as surrogate marker for RNA valency.

B. RNA-FISH (white) of mRNAs from the indicated transfected constructs in HeLa cells before (-) and after (+) digitonin extraction. DAPI (blue) stains nuclei. Thin yellow dashed lines indicate cell boundaries, and thick dotted lines mark the nucleus. As digitonin only extracts cytoplasmic mRNAs, only cytoplasmic RNA-FISH signal was analyzed. Representative images are shown.

C. Quantification of (B). Fraction of digitonin-resistant mRNA in the cytoplasm shown as mean ± SEM from $N = 3$ independent experiments. The number of analyzed cells is shown. Mann-Whitney test: ****, $P < 0.0001$.

D. As in (B), but RNA-FISH was performed on *KDM6B* mRNA with swapped 3′UTRs. Constructs shown in Fig. 5A.

E. Western blot showing TIAL1 expression in a doxycycline inducible CRISPR/Cas9 HeLa cell line expressing either gRNAs targeting TIAL1 (iKO) or non-targeting control (Ctrl). GAPDH was used as the loading control.

F. As in Fig 1L, but JMJD3 cellular activity in Ctrl or *TIAL1* iKO HeLa cells after transfection of the HA-KDM6B-U construct.

G. As in Fig. 1M, but JMJD3 protein abundance of transfected full-length JMJD3 in the indicated cell lines from $N = 3$ independent experiments is shown. Mann-Whitney test: $P = 1.9 \times 10^{-10}$.

Figure S7

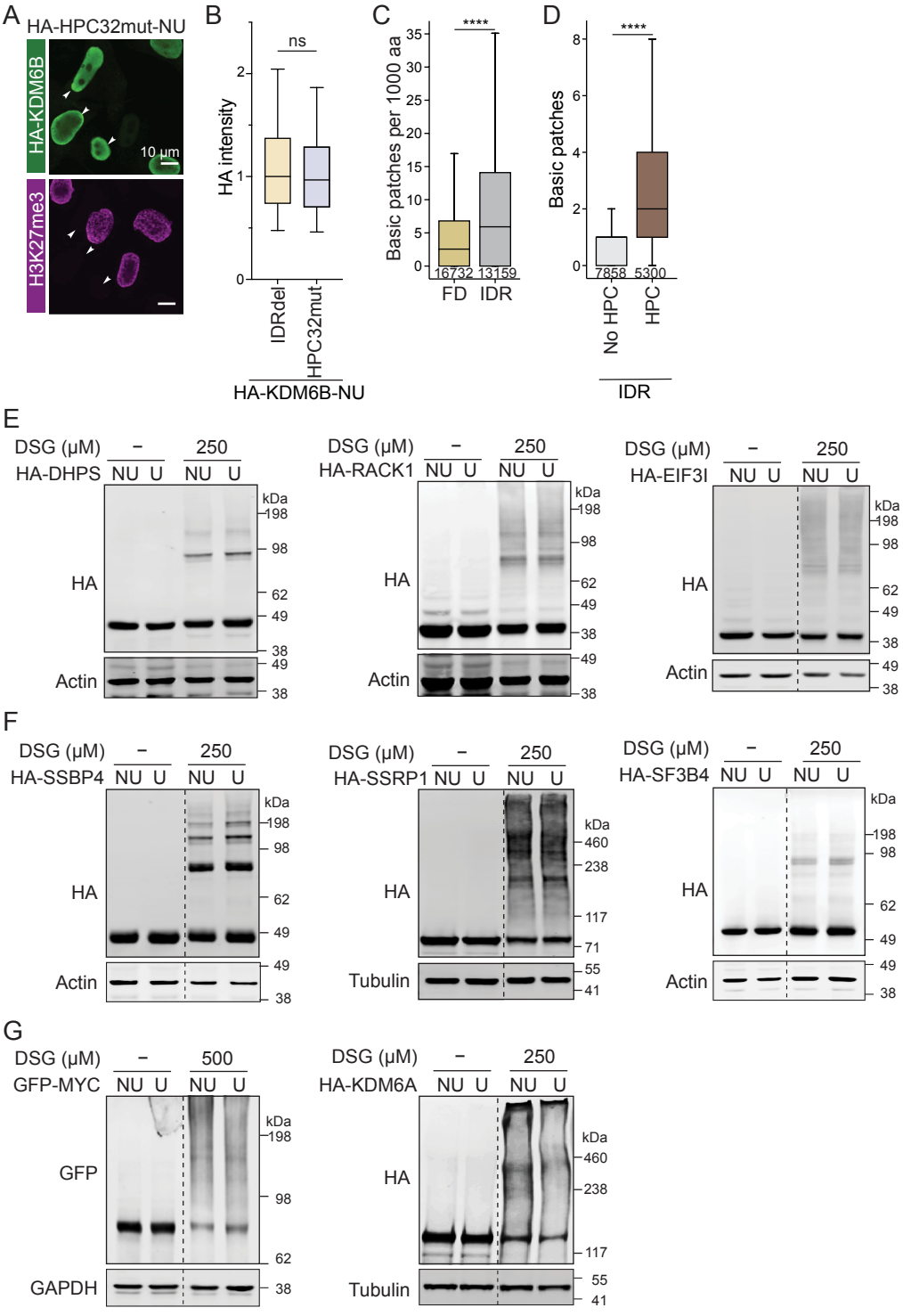
A
HA-HPC32mut-NU
HA-KDM6B
H3K27me3
10 µm
B
HA intensity
ns
IDRdel
HPC32mut
HA-KDM6B-NU
C
Basic patches per 1000 aa
****
16732
13159
FD
IDR
D
Basic patches
****
7858
5300
No HPC
HPC
IDR
E
DSG (µM) – 250
HA-DHPS NU U NU U
HA-RACK1 NU U NU U
HA-EIF3I NU U NU U
HA
Actin
kDa
198
98
62
49
38
F
HA-SSBP4 NU U NU U
HA-SSRP1 NU U NU U
HA-SF3B4 NU U NU U
460
238
117
71
Tubulin
55
41
G
DSG (µM) – 500
GFP-MYC NU U NU U
GFP
GAPDH
DSG (µM) – 250
HA-KDM6A NU U NU U

Figure S7. Protein crosslinking patterns of IDR-containing proteins with hydrophobic clusters change in a 3′UTR-dependent manner, related to Figure 6 and 7

A. As in Fig. 1L, but JMJD3 cellular activity in HeLa cells after transfection of the HP32Smut construct.

B. As in Fig. 1M, but JMJD3 protein abundance of the IDRdel and HP32Smut constructs was measured as HA intensity from *N* = 3 independent experiments. Mann-Whitney test: ns, not significant.

C. Basic patches per 1000 amino acids in the longest folded domains (FD, *N* =16732) vs the longest IDRs (*N* = 13159) in each protein. Mann-Whitney test: $P = 1.6 \times 10^{-236}$.

D. As in Fig. 6E, but the number of basic patches is shown. IDR-containing proteins *N* = 13159, IDRs with HP clusters, *N* = 5300, and IDRs without HP clusters, *N* = 7858. Mann-Whitney test: ****, *P* = 0.

E-G. Protein crosslinking patterns in cells after transfection of the indicated HA-tagged constructs were analyzed by DSG cross-linking and western blot analysis. The dotted lines refer to the removal of irrelevant lanes from the image of the blot.

E. DSG crosslinking western blot of HA-tagged folded proteins shows 3′UTR-independent protein crosslinking patterns. Actin was used as loading control.

F. As in (F) but shown are HA-tagged IDR-containing proteins free of HP clusters. Actin or Tubulin were used as loading controls.

G. DSG crosslinking western blot of HA-tagged proteins containing IDRs with HP clusters shows 3′UTR-dependent protein crosslinking pattern. GAPDH or Tubulin were used as loading controls.